JOURNAL OF SPACECRAFT AND ROCKETS
Vol. 47, No. 5, September–October 2010

Near-Ultraviolet Spectroscopy of the Stardust Sample Return Capsule Reentry

Richard L. Rairden*
Lockheed Martin Advanced Technology Center, Palo Alto, California 94304
and
Peter Jenniskens†
SETI Institute, Mountain View, California 94043

DOI: 10.2514/1.40440

The 320–460 nm wavelength emission of the Stardust Sample Return Capsule's reentry in Earth's atmosphere was observed remotely with an intensified slitless spectrograph, which recorded spectra at a video rate of 29.97 frames/s. The spectral response remained constant during the full range of recovery, with only motion blurring from imperfect guiding contributing to small variations in detection response. The data are well suited for evaluating the temporal variation of the intensity of the various light-emitting components. A line of zinc identifies the period when a layer of ZnO pigment containing thermal protection paint was ablated. Ca^+ emission was more intense during (and just following) the ablation of this zinc, but present throughout flight. Shock emission from nitrogen is no longer detected shortly after peak heating. The data are dominated by strong molecular band emission from the radical CN. The CN band intensity is thought to be proportional to the carbon ablation rate from the heat shield. Corrected for distance, the CN band intensity peaked early in flight, before peak heating, followed by an exponential decrease through peak heating.

I. Introduction

THE fast 12.8 km/s entry of the Stardust Sample Return Capsule in Earth's atmosphere was the first system field test of a phenol-impregnated carbon ablator (PICA) thermal protection system. At the time, PICA was considered a potential material of choice for the thermal protection system of NASA's next generation of spacecraft [1].

The carbon atoms ablating from the heat shield react with the atmospheric nitrogen molecules to create CN radicals, which shine brightly at near-UV wavelengths around 388 nm [2,3]. In that same wavelength range, the isoelectric N_2^+ molecule also emits molecular band emission, slightly offset from that of CN, with a band head at 391 nm. Weak N_2^+ emission was predicted in preflight radiation calculations of the shock emission ([1], Fig. 6).

NASA's DC-8 Airborne Laboratory was deployed to observe the reentry above the weather, with a low and well-defined telluric extinction in the line of sight from capsule to observer [4]. The aircraft was equipped with fused quartz windows, which are transparent in the wavelength range above the atmospheric cutoff at ~300 nm from ozone absorption.

Here, we report on time-resolved low-resolution near-UV observations of the capsule's radiation in the range 320–460 nm, using an intensified slitless spectrometer. The same camera was used in past meteor shower observing campaigns [5,6]. These data may be used for studies of the carbon ablation rate throughout flight.

II. Methods

The camera consisted of a *Noctron* UV-sensitive image intensifier of Aspect Technology & Equipment, Inc., equipped with a UV-Nikkor 105 mm $f/4.5$ objective lens, and a 600 lines/mm diffraction grism mounted in front of the objective lens. The intensifier was optically coupled to a Pulnix model TM-745 NTSC video camera head. The video signal was routed through a TrueTime video time inserter to stamp IRIG time data onto the video frames, and then recorded on Digital 8 cassette tape using a Sony DCR-350. The camera had a field of view of 8×11 degrees and gave a better than 2 nm resolution in first order over the wavelength range from 320 to 460 nm.

The camera, called IUV, was mounted in a coaligned manner below a second near-UV camera, called NUV, behind a fused quartz aircraft window. The pointing was achieved by the operators of the NUV camera, using an additional coaligned intensified camera. The pointing of IUV relative to NUV was calibrated on distant tarmac lights before flight. The window transmission is virtually constant over the full wavelength range. The response of the camera and transparency of the window was tested in a laboratory setting. The first-order spectral dispersion was 0.394 nm per pixel. The instrumental broadening was measured from the camera response to stars and from laboratory measurements to the response of emission line calibration lamps. The full-width at half-maximum of the instrument convolution function equals 1.9 nm or about 5 pixels.

For analysis, the video images are digitized as 640×480 pixel arrays at 8-bit resolution. Figure 1 shows a typical example. The zero-order image of the capsule is ~17 deg below, right outside the field of view. By extracting a band of pixel intensities, one-dimensional spectra are obtained as shown in Fig. 2.

The relative responsivity was measured by comparing the mean IUV data for the 1 s interval centered on 09:57:25.5 UTC (Coordinated Universal Time), after correction for atmospheric extinction in the line of sight, to the independently reduced data of the echelle-based spectrograph for the crisp and high efficient detection of low light emission (called ECHELLE) [7] and the slit-based spectrometer (called SLIT) [8]. The instrumental response (Fig. 3) is nearly flat and mostly a function of the intensifier response, given that the lens and quartz window have good throughput throughout the 320–460 nm wavelength range. The cathode radiant sensitivity (mA/W) of a bialkali intensifier, scaled to the measured responsivity, is shown by a dashed line in Fig. 3. At short and long wavelengths, instrumental vignetting, typically proportional to $\cos^4(\alpha)$, where α is the viewing angle away from the image center, lowers the responsivity slightly. A good fit to the response curve is obtained by a function

Received 15 August 2008; revision received 12 April 2010; accepted for publication 27 April 2010.

*Senior Staff Physicist, 3251 Hanover Street, Dept. ADCS, Building 255; rick.rairden@lmco.com. Senior Member AIAA.

†Carl Sagan Center, 515 North Whisman Road; Petrus.M.Jenniskens@nasa.gov.

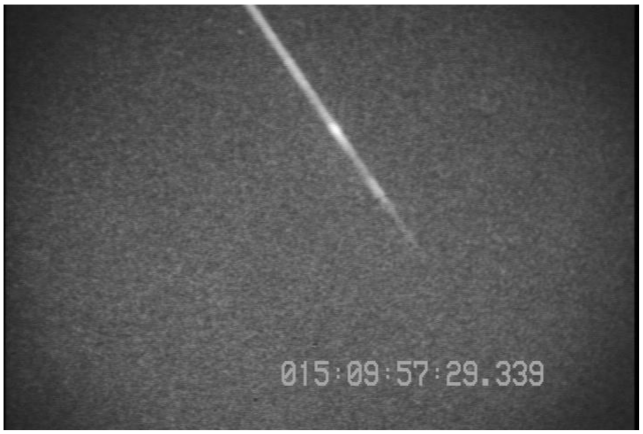

Fig. 1 Example video frame in the near-UV spectrum. Such spectra are extracted from 1131 sequential frames and stacked to left to right in Fig. 4 to show the intensity as a function of time.

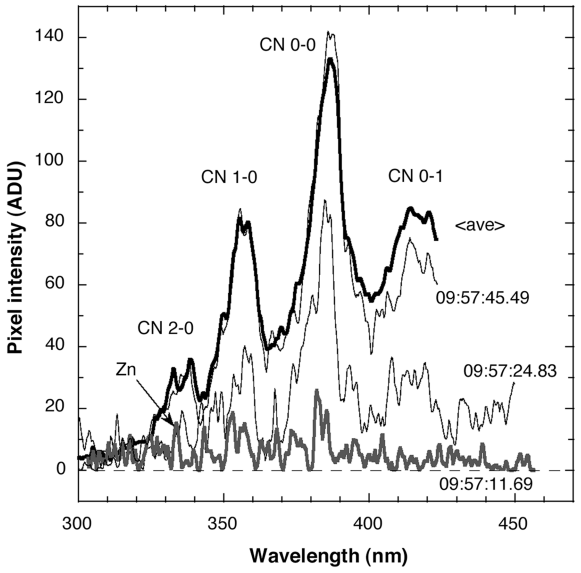

Fig. 2 Typical extracted spectra during the reentry. Single-frame spectra are time-tagged. The bold profile is an average of several frames around peak heating. The intensity scale here is uncalibrated.

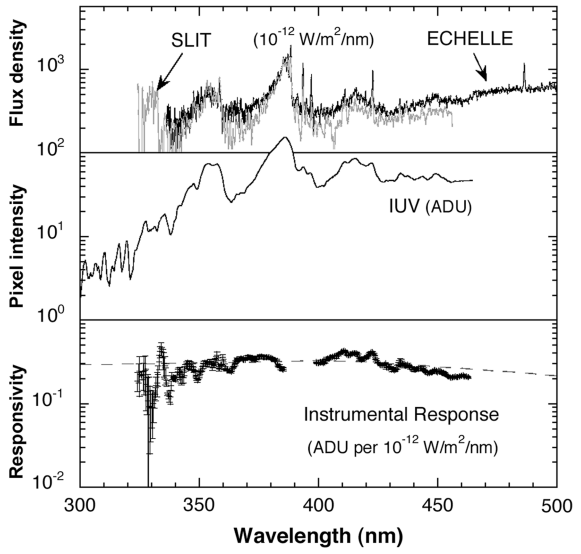

Fig. 3 Instrumental response curve derived from comparing average IUV data for the 1 s interval centered on 09:57:25.5 UTC to those of ECHELLE [7] and SLIT [8]. Dashed line is the cathode radiant sensitivity of a bialkali intensifier, scaled to the measured response data.

$f(\text{ADU per } 10^{-12}\ \text{W/m}^2/\text{nm}) = 0.36 \times \cos^4((\alpha(\text{nm}) - 400)/2.0)$
where ADU is the analog-to-digital unit.

Because the spectrum is recorded in slitless mode, the response of the instrument does not vary as a function of time. This makes these data suitable for studies of temporal variation of spectral features, more so than slit spectra [6]. The only variables are the atmospheric extinction between observer and capsule, and the distance to the capsule.

III. Results

Figure 4 contains the spectra from 1131 images, stacked in time order from the left at 09:57:11.186 to the right at 09:57:48.891 UTC, covering 37.705 s of video data at 29.97 frames per second. The wavelength increases from about 290 nm at the bottom to 460 nm at the top. Atmospheric extinction effectively truncates the observations below 320 nm. The edge of the hand-guided camera field of view truncates the longer wavelength end of the spectra. Shorter wavelengths are also truncated (lower right corner) during the final 2 s, when the trajectory exceeded our tracking limit and passed behind the window frame.

This intermediate data summary was achieved using an IDL (Interactive Data Language, software by Research Systems, Inc.) routine that reads each image, finds the spectrum, and then registers the spectral profile to line up the maximum peak. The spectra have the background level as defined by the rest of the frame subtracted, where the background level is taken as a profile displaced 10 pixels off the spectrum. Noise is reduced by taking each profile as a sum of five-pixel rows. Initially, there were darker vertical lines that looked like dropped spectra, which were due to frames where the camera guiding was irregular and resulted in blurred spectra. These blurry spectra were renormalized to the intensity of neighboring spectra that were not broadened by motion blurring.

Saturated pixels are considered to have intensity as measured, and no correction was made to take saturation into account. The strongest emission feature in the data, the 388 nm CN ($\Delta\nu = 0$-0) band, saturated in the center of the band only after time 09:57:30.2 UTC. The other $\Delta\nu = 1$-0 and 0-1 CN bands did not saturate.

The dominant molecular bands in this data set are from CN radicals, not from N_2^+. Other instruments, such as ECHELLE [7], resolved the two band heads at 388 and 391 nm and showed that N_2^+ is at least an order of magnitude less intense than the isoelectric CN band in this wavelength range. The instrument-broadened molecular bands are centered on 357, 386, and 417 nm. The CN band emission increases monotonically until after peak heating (Fig. 4).

From the very beginning of the observation at 09:57:11 UTC, strong lines of Zn were identified by other instruments [7]. These strong zinc lines at 468–481 nm are just out of range of our instrument. However, other lines of zinc were detected at 330.3535 and 334.5977 nm (vacuum wavelengths from the Kurucz Atomic Line Database [10]). These lines are well discriminated from the $\Delta\nu = 2$-0 CN band, because they are strong only over a short interval of time. The zinc signature at 330–335 nm does not persist past the point where the signal is initially lost, and intensity at this wavelength later in the range is from features of the $\Delta\nu = 2$-0 CN band (Figs. 2 and 4).

Two atomic lines of singly ionized calcium (Ca^+) are also present. They are detected starting at around 09:57:17 UTC, strongest between 09:57:20 and 09:57:24 UTC, but they are seen faintly throughout the entire range. The early Ca^+ peak follows the ablation of the zinc. This suggests that calcium is an impurity in both the paint layer and the PICA. A line at 422 nm is perhaps due to neutral calcium.

In many other observations onboard the DC-8 Airborne Laboratory, the air plasma emission from the shock wave was seen to disappear just after peak heating. Indeed, the peak around 415 nm has this behavior and we suspect that this is a line from atomic nitrogen.

The spectra also contain continuum emission from the hot thermal protection system surface. The continuum emission is mostly isolated from the CN bands above 430 nm.

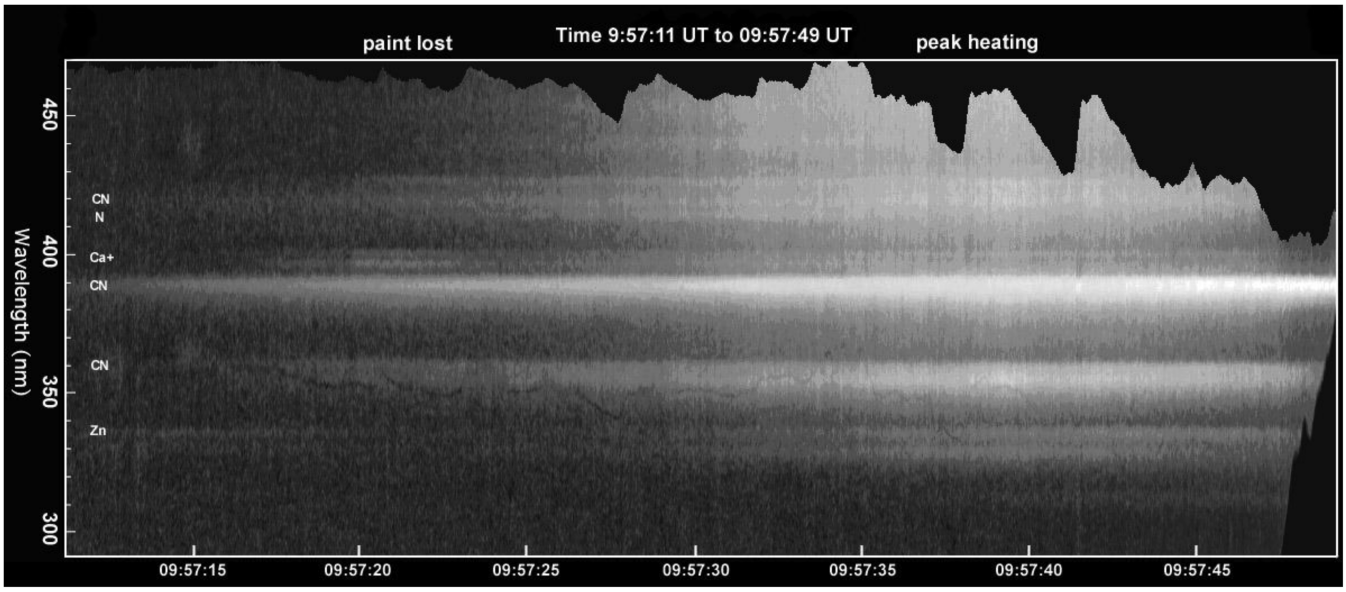

Fig. 4 Temporal variation of the recorded UV spectra, each pixel column depicting the extracted one-dimensional spectrum in consecutive video frames spanning 37.7 s (left to right). The pixel intensity is uncalibrated for instrument response or extinction.

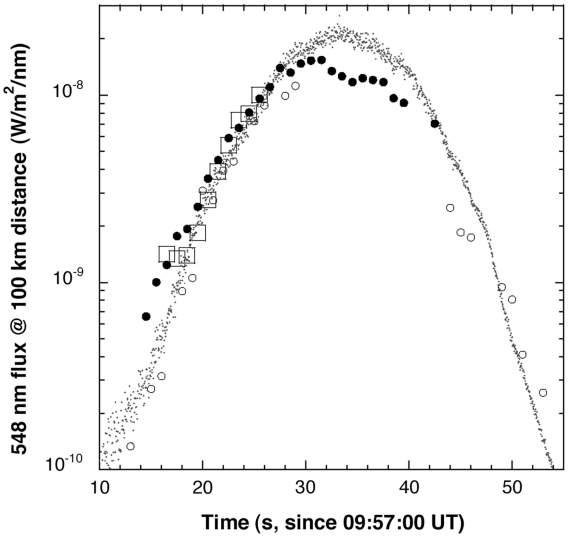

Fig. 5 Temporal variation of the continuum emission intensity at 548 nm. The IUV data (●, small) are compared to those of a low-light-level TV-pointing camera (+) [12], the DIM digital photographs (○, large) [11], and the ECHELLE spectroscopy (square) [7].

IV. Discussion

These data are now available for analysis. For example, Fig. 5 shows the temporal variation of the continuum emission intensity. The results are compared to those of other cameras, and all measurements were translated to a flux at 548 nm (peak of the visual Johnson V-band filter). We also corrected the observed flux measurements toward a standard distance of 100 km [9]. This makes it possible to see when the entry radiation was peaking.

The measured continuum at 445 nm was corrected to that expected at 548 nm, assuming a blackbody emission and an approximate surface temperatures derived from theoretical models. This correction amounted to a factor of 6.4 at 09:57:11 UTC, decreasing to 2.15 at 09:57:34 UTC, before increasing to 2.31 at 09:57:46 UTC. The resulting shape of the curve (Fig. 5) is in good agreement with unsaturated data from ECHELLE (open squares) and DIM (digital imager, filled circles). The IUV data are not independently calibrated, but rather scaled to the ECHELLE [7] and DIM [11] flux measurements at 09:57:22-25 UTC (Fig. 5).

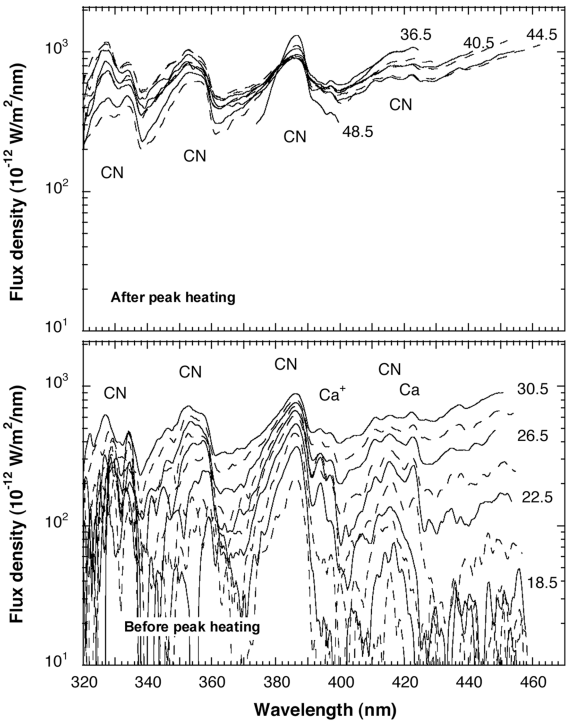

Fig. 6 Fully calibrated data, showing the temporal variation of the CN band intensity. Each line is a 1 s average, and only even seconds are shown.

The peak radiation occurred around 09:57:30.5 UTC, at the predicted time of peak heating [1]. The surface temperature did not change much from 09:57:29 until 09:57:32 UTC. Following peak heating, there was a gradual decline of surface radiation at 548 nm. The IUV data trace this behavior well because the dispersion of light in a first-order spectrum prevented saturation of the data. The three DIM data points around 09:57:45 UTC are saturated.

As a second example of how these data may be applied, we show in Fig. 6 the temporal variation of the CN band intensity in calibrated data. The flux given is the apparent flux density just outside the aircraft, after correction for telluric extinction. The apparent flux density of the $\Delta\nu = 1$-0 and 0-1 bands only slightly decreased after peak heating, at least until 09:57:48.5 UTC. During this time frame,

the $\Delta v = 0$-0 band was saturated. Corrected for distance, the CN band intensity peaked early in flight, before peak heating, followed by an exponential decrease through peak heating. The necessary comparison to theoretical models in order to interpret these data in terms of ablation rates is beyond the scope of this paper.

V. Conclusions

Low-resolution spectra were obtained in the 320–460 nm wavelength range. The extracted spectra provide an accurate record of the temporal variation of emission features, which are related to the ablation rate of white paint, the ablation rate of PICA, and the surface temperature of the Stardust Sample Return Capsule.

The results are available now for interpretation. The observations of the Stardust Sample Return Capsule entry are expected to remain a unique system field test for a long time to come. The observational data will be archived for this purpose. The present paper serves to document the files in hand.

Acknowledgments

NASA's DC-8 Airborne Laboratory was deployed by the University of North Dakota and National Suborbital Education and Research Center, under contract with NASA Wallops Flight Center. This work was funded and managed by the Orion Thermal Protection System Advanced Development Project and the NASA Engineering and Safety Center.

References

[1] Jenniskens, P., Kontinos, D., Jordan, D., Wright, M., Olejniczak, J., Raiche, G., et al., "Preparing for the meteoric return of Stardust," *Dust in Planetary Systems*, edited by A. Grapps, and E. Gruen, Vol. 643, ESA, Paris, 2006, pp. 7–10.

[2] Hoshizaki, H., and Lasher, L. E., "Convective and Radiative Heat Transfer to an Ablating Body," *AIAA Journal*, Vol. 6, No. 8, 1968, pp. 1441–1449. doi:10.2514/3.4786

[3] Wilson, K. H., and Hoshizaki, H., "Effect of Ablation Product Absorption and Line Transitions on Shock Layer Radiative Transport," NASA CR-1264, 1969.

[4] "Stardust Hypervelocity Entry Observing Campaign Support," NASA Engineering and Safety Center Rept. RP-06-80, Aug. 2006.

[5] Rairden, R. L., Jenniskens, P., and Laux, C. O., "Search for Organic Matter in Leonid Meteoroids," *Earth, Moon, and Planets*, Vol. 82–83, 2000, pp. 71–80. doi:10.1023/A:1017021929075

[6] Jenniskens, P., and Rairden, R. L., "Buoyancy of the Y2K Persistent Train and the Trajectory of the 04:00:29 UT Leonid Fireball," *Earth, Moon, and Planets*, Vol. 82–83, 2000, pp. 457–470. doi:10.1023/A:1017044229442

[7] Jenniskens, P., "Observations of the Stardust Sample Return Capsule Entry with a Slitless Echelle Spectrograph," *Journal of Spacecraft and Rockets*, Vol. 47, No. 5, 2010, pp. 718–735. doi:10.2514/1.37518

[8] Winter, M., and Herdrich, G., "Spectroscopic Observation of the Stardust Re-Entry in the Near UV," AIAA Paper 2007-4050, Miami, FL, June 2007.

[9] Levit, C., "Reconstruction and Verification of the Stardust SRC Re-Entry Trajectory," AIAA Paper 2008-1199, Reno, NV, Jan. 2008.

[10] Kurucz, R. L., and Bell, B., *Kurucz 1995 Atomic Line Data* [CD-ROM], No. 23, Smithsonian Astrophysical Observatory, Cambridge, MA, 1995.

[11] Jenniskens, P., and Wercinski, P., "Digital Still Snapshots of the Stardust Sample Return Capsule Entry," *Journal of Spacecraft and Rockets* (to be published).

[12] McHarg, M. G., and Stenbaek-Nielsen, H. C., "Observations of the Stardust Sample Return Capsule Entry Using a High Frame Rate Slitless Spectrograph," AIAA Paper 2008-1211, Reno, NV, Jan. 2008.

D. Kontinos
Guest Editor